J Biomol NMR (2015) 63:245–253
DOI 10.1007/s10858-015-9980-1

ARTICLE

Asynchronous through-bond homonuclear isotropic mixing: application to carbon–carbon transfer in perdeuterated proteins under MAS

Natalia Kulminskaya[1] · Suresh Kumar Vasa[1] · Karin Giller[1] · Stefan Becker[1] · Rasmus Linser[1]

Received: 27 May 2015 / Accepted: 24 August 2015 / Published online: 30 August 2015

Abstract Multiple-bond carbon–carbon homonuclear mixing is a hurdle in extensively deuterated proteins and under fast MAS due to the absence of an effective proton dipolar-coupling network. Such conditions are now commonly employed in solid-state NMR spectroscopy. Here, we introduce an isotropic homonuclear ^{13}C–^{13}C through-bond mixing sequence, MOCCA, for the solid state. Even though applied under MAS, this scheme performs without rotor synchronization and thus does not pose the usual hurdles in terms of power dissipation for fast spinning. We compare its performance with existing homonuclear ^{13}C–^{13}C mixing schemes using a perdeuterated and partially proton-backexchanged protein. Based on the analysis of side chain carbon–carbon correlations, we show that particularly MOCCA with standard 180-degree pulses and delays leading to non-rotor-synchronized spacing performs exceptionally well. This method provides high magnetization transfer efficiency for multiple-bond transfer in the aliphatic region compared with other tested mixing sequences. In addition, we show that this sequence can also be tailor-made for recoupling within a selected spectral region using band-selective pulses.

Keywords SH3 domain · Solid-state NMR (ssNMR) · MAS · Homonuclear isotropic mixing · Perdeuterated proteins · MOCCA

Introduction

An increasing number of methods enabling the effective use of proton-detected solid-state NMR spectroscopy have been developed in recent years as a potent complement to the traditional set of ^{13}C-detected methods. (Knight et al. 2012; Linser et al. 2011b) This is possible due to the development of dedicated proton-dilution techniques (Agarwal et al. 2006; Asami et al. 2010; Chevelkov et al. 2006; McDermott et al. 1992; Morcombe et al. 2005) and has been much facilitated by faster Magic-Angle-Spinning (MAS) technology (Agarwal et al. 2014; Knight et al. 2011; Lewandowski et al. 2011). Both effectively reduces the destructive influence of proton–proton dipolar couplings and has enabled new strategies towards unambiguous resonance assignments (Knight et al. 2011; Linser et al. 2011b), protein structure determination (Agarwal et al. 2006; Huber et al. 2011; Knight et al. 2012; Linser et al. 2011a, 2014), and the elucidation of atom-specific protein dynamics and interactions (Chevelkov et al. 2009; Lamley et al. 2014; Linser et al. 2009; Schanda et al. 2010). Importantly, the usage of methodology derived from solution NMR spectroscopy has become available also in the solid state, i.e. omission of high-power decoupling, exploitation of scalar transfers (Linser et al. 2008, 2010) and differential relaxation (Chevelkov et al. 2007; Linser et al. 2010), and fast-recycling techniques (Linser et al. 2007). At the recent state of hardware development, reduction of the effects of the proton dipolar-coupling network is mostly effected by utilization of aliphatic

Electronic supplementary material The online version of this article (doi:10.1007/s10858-015-9980-1) contains supplementary material, which is available to authorized users.

✉ Rasmus Linser
rali@nmr.mpibpc.mpg.de

[1] Department of NMR-based Structural Biology, Max Planck Institute for Biophysical Chemistry, 37077 Göttingen, Germany

deuterons in combination with proton back-exchange of amide sites (Barbet-Massin et al. 2014) or specific (sparse) introduction of methyl protons (Huber et al. 2012) or aliphatic protons in general (Asami et al. 2015). Higher proton dilution and faster MAS have commensurate effects. This leads to similar sensitivities of larger rotor volumes with higher dilution and smaller rotors with lower dilution. Thus, within limits, overall costs can often be reduced by choosing a smaller rotor size.

The absence of an effective proton dipolar-coupling network goes in hand with the unavailability of traditional carbon–carbon mixing schemes like proton-driven spin diffusion (PDSD) (Bloembergen 1949) and dipolar-assisted rotational resonance DARR (Takegoshi et al. 2001). Taking into account deuterons for carbon mixing (Akbey et al. 2009) has been suggested to aid in carbon–carbon correlations but requires the probe to offer a fourth (deuterium) channel. Alternatively, homonuclear recoupling sequences like radio-frequency driven recoupling (RFDR) (Bennett et al. 1992, 1998; de Boer et al. 2004), HORROR (Nielsen et al. 1992), or similar would be possible alternatives. In contrast to the benefits with respect to alleviating the detrimental effects of proton dipolar couplings, however, fast MAS also renders the employment of rotor-synchronized recoupling sequences increasingly difficult: This is mostly due to a shorter time window for radio-frequency pulses generally (more frequent, higher-power pulses). Additionally, there is often a necessity for effective fields, for example in symmetry-based sequences, of at least 2–3 times the rotor frequency (Brinkmann et al. 2000; Carravetta et al. 2000; Hou et al. 2012; Kristiansen et al. 2006). Both leads to increased deposition of energy and easily exceeds the limits of protein samples and probes. Also lower-power symmetry-based mixing schemes (Nielsen et al. 2011; Teymoori et al. 2013) for homo- and heteronuclear correlations have been demonstrated using either composite pulses (Hardy et al. 2001) or phase-modulated pulses based for example on advanced genetic algorithms (Herbst et al. 2011; Bellstedt et al. 2012). However, continued development and improvements regarding robust schemes for low-power recoupling over multiple bonds that are easy to set up for different spinning speeds are currently needed.

Owing to the reduced effects of proton dipolar coupling under fast-spinning conditions, particularly in combination with proton dilution with deuterium, we figured that new strategies should be possible to achieve low-power mixing of magnetization among heteronuclei. Concomitant decoupling of proton dipolar couplings is not required. Hence, solution-NMR isotropic mixing schemes should be feasible that are based on introduction of *J*-couplings by the help of dedicated multiple-pulse sequences.

Mixing schemes like TOCSY (Grzesiek and Bax 1995), FLOPSY (Kadkhodaie et al. 1991), and MOCCA (Modified phase-Cycled Carr-Purcell) (Felli et al. 2009; Kramer et al. 2001; Yoshimura et al. 2015) can potentially represent a critical challenge for hardware and temperature stability in the solution state. However, they seem to be a less significant challenge in solid-state NMR measurements: For the rf fields required for solution-NMR mixing schemes, both hardware sensitivity and temperature changes over time or gradients over the sample can be expected to be relatively unproblematic in comparison to traditional solid-state NMR sequence elements. Also, another challenge in the solution state, achieving sufficiently broadband mixing, is expected to be less of a problem with the more powerful solid-state amplifiers. More importantly, non-rotor-synchronized *J*-coupling mixing schemes are independent of any MAS frequency, i.e., their power requirements do not generally scale up with increasing ν_r, as long as unwanted recoupling effects during the hard pulses are prevented.

Here we address the problem of isotropic mixing between like spins for intra-residual ^{13}C–^{13}C connectivites, especially sidechain to backbone magnetization transfer. Several sequences in this vein have been described for both protonated as well as for perdeuterated proteins (Bennett et al. 1992, 1998; Bloembergen 1949; de Boer et al. 2004; Hardy et al. 2001; Leppert et al. 2004; Nielsen et al. 1992; Takegoshi et al. 2001; Verel et al. 1998, 2001). In the following, we evaluate how mixing can be achieved for perdeuterated rotating solids at 25 kHz spinning with high magnetization transfer efficiency. In this work, we demonstrate the through-bond homonuclear mixing sequence MOCCA for the solid state. Previously, MOCCA was successfully employed in liquid-state NMR (Felli et al. 2009; Kramer et al. 2001; Yoshimura et al. 2015) as an isotropic scalar-coupling-based mixing sequence. In the liquid state, improvements have been described for a modified phase-cycled Carr-Purcell multiple-pulse scheme with various super cycles. This owes to reduced relaxation loss upon minimization of the detrimental impact of pulse imperfections of the 180° pulses (Kramer et al. 2001).

In solid-state NMR under MAS conditions, application of delays between the pulses in a non-rotor-synchronized fashion allows the MOCCA hard-pulse sequence to achieve long mixing times and results in long-distance magnetization transfer without heating of the sample. This significantly reduces the risk of compromising the probe integrity at high spinning speeds. It can be applied using hard pulses and soft pulses, depending on which nuclei are to be recoupled. We compare its performance with the mixing sequences RFDR (Bennett et al. 1992, 1998) and TOBSY (Baldus and Meier 1996; Hardy et al. 2001; Leppert et al. 2004) using perdeuterated SH3 domain of chicken α-

spectrin at 25 kHz spinning in the absence of proton decoupling.

Materials and methods

Sample preparation

Protein samples of the SH3 domain of α-spectrin were prepared as described previously (Linser et al. 2007) using 30 % ^{1}H back substitution of amide protons, respectively, in otherwise deuterated, ^{13}C and ^{15}N-labeled protein. Paramagnetic doping was applied as described previously using 75 mM $[Cu^{II}(edta)]_2$— (Linser et al. 2007) For the NMR measurements, approximately 3 mg of the protein were centered in a 2.5-mm thick-wall rotor using spacers in the top and bottom of the rotor.

ssNMR experiments and analysis

All NMR experiments were performed at a sample temperature of 288 K on a Bruker Avance NMR spectrometer at ^{1}H frequency of 400 MHz equipped with a wide-bore 2.5-mm HCN triple-resonance magic angle spinning probe. Unless otherwise stated, all spectra were recorded at 25 kHz spinning speed, and 4,4-dimethyl-4-silapentane-1-sulfonic acid (DSS) was used as a standard for chemical shift referencing. The spinning speed was regulated by a BRUKER MAS controller with a variation in the spinning speed of around ±5 Hz. A 90° hard pulse of 2.5 µs (100 kHz) and 6.25 µs (40 kHz) was applied on ^{1}H and ^{13}C channels, respectively. For Hartmann–Hahn CP, the n = +1 condition was used with rf field strengths of 65.8 and 42.9 kHz on the ^{1}H and ^{13}C channel, respectively, with a 100–90 % ramped CP pulse on the ^{1}H channel. The CP contact time was set to 600 µs. For all comparison experiments, these parameters were kept constant. For MOCCA with soft pulses, the radiofrequency field of the 180° pulses was set to 9.2 kHz with a duration of the 180° pulses of 60 µs, which was optimized such that ^{13}C′ nuclei experience an effective 360° rotation during each ^{13}Cα 180° pulse (Felli et al. 2009). For hard-pulse MOCCA, we used 10.5 µs 180-degree pulses, corresponding to 47.6 kHz B_1. 2D correlation spectra were acquired with a spectral width of 355 ppm in the direct dimension and 198 ppm with 320 time increments in the indirect dimension, resulting in total acquisition times of 15 and 8 ms for the direct and indirect dimension, respectively. Unless otherwise stated, all experiments were recorded in 3 h each. All NMR data were processed using TopSpin 3.2 software and subsequently analyzed using Sparky (Goddard and Kneller). TOBSY isotropic mixing (Baldus and Meier 1996; Hardy et al. 2001; Leppert et al. 2004) was implemented as described elsewhere (Agarwal and Reif 2008; Linser 2011), with the optimized pulse duration of 28 µs and using an effective field of 37 kHz and various mixing times.

Results

Our results show that intra-residual connectivities between the backbone and the various side-chain carbons can be established in the solid state using the MOCCA isotropic mixing scheme in a non-rotor-synchronized fashion. Figure 1a depicts the pulse scheme we employed for characterizing the performance of various mixing schemes for 2D carbon–carbon correlation experiments. Briefly, after the direct excitation of ^{13}C, cross-polarization (CP) from protons to carbons is used. This provides additional magnetization of sidechain carbons at the starting point according to the COPORADE approach (Linser 2011), followed by frequency encoding in the indirect ^{13}C dimension. Combined single pulse and CP are significantly improving the s/n for all carbons in the sidechain (Linser 2011) and allowed us to work with higher initial magnetization (particularly for carbons distant from H^N) prior to mixing, compared to each individual source of carbon excitation. After frequency encoding, carbon magnetization is flipped to the z-axis, homonuclear mixing is applied and the signal

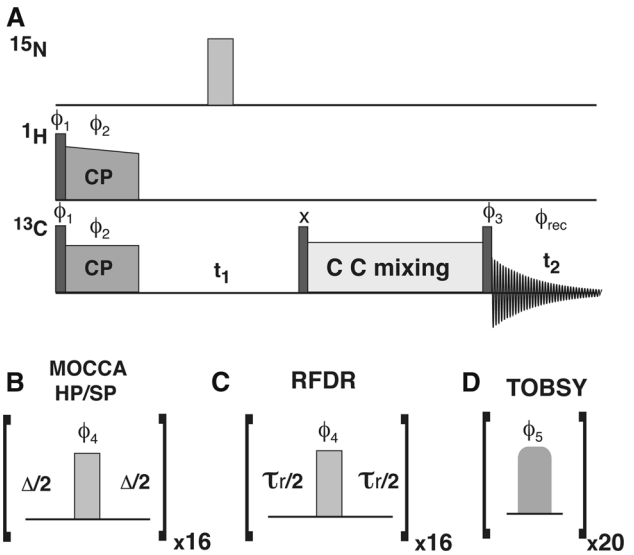

Fig. 1 **a** Schematic representation of the pulse sequence used for the 2D ^{13}C–^{13}C correlation experiments with various homonuclear mixing sequences **b** MOCCA **c** RFDR **b** TOBSY. Narrow bars represent hard 90-degree pulses, whereas *wide bars* represent 180-degree pulses. Their corresponding phases are listed on top with the following phase cycle: ϕ_1 = 0°, 180°; ϕ_2 = 90°, 270°; ϕ_3 = 90°, 90°, 270°, 270°; ϕ_4 = 180°, 0°, 180°, 0°, 0°, 180°, 0°, 180°, 90°, 270°, 90°, 270°, 270°, 90°, 270°, 90°; ϕ_5 = 0°, 240°, 240°, 60°, 0°, 0°, 240°, 240°, 60°, 0°, 180°, 60°, 60°, 240°, 180°, 180°, 60°, 60°, 240°, 180°; ϕ_{rec} = 180°, 0°, 0°, 180°

finally detected in the direct dimension after a 90° read-out pulse.

To find the optimal transfer efficiency of hard-pulse MOCCA, we recorded a series of 2D ^{13}C–^{13}C correlation experiments. In a first step, we optimized the hard 180° pulse in a 1D fashion. Then, varying the delay Δ between the pulses using a fixed hard 180° pulse duration (of 10.5 μs), we found identical optimized conditions for maximum magnetization transfer for one, two, and three-bond transfers at the same time. Resulting optimization curves for various cross peaks are shown in Fig. 2 (and Figure S3 of the Supporting Information) for a fixed total mixing time of 15 ms. Each 2D spectrum was recorded in 3 h, which prohibited a finer grid or more accurate measurements. The profiles shows clear maximum conditions for 40, 60, and 100 μs, interrupted for example by poor performance at 50 μs (rotary resonance condition with $\Delta + \tau_{180°} = 1.5\tau_r$). In the course of Δ variation, we covered dipolar-recoupling conditions such as $\Delta + \tau_{180°} = 1\tau_r$, $2\tau_r$, $3\tau_r$ and $4\tau_r$ (black dashed lines in Fig. 2 marking $\Delta + \tau_{180°} = n\tau_r$), which provide significantly lower intensity compared to the favorable condition. This behavior clearly deviates from rotor-synchronized mixing, which suggests that the sequence maintains its character of a through-bond isotropic mixing scheme. A finer optimization of the delay around the maximum (with Δ being around 60 μs) was performed thereafter, see the corresponding intensity profile in Figure S5. The cross peak intensities of various residues clearly show that the optimal conditions for the delay, Δ, are narrow. This profile is similar to the 1D optimization profile for the delay with different loop counters (Figure S6). Efficient optimization of the delay around 60 and 100 μs turned out to be achievable upon variation of Δ in such 1D experiments with a 0.5–1 μs step size and employing the values with maximum overall intensities within those regions (see Figure S6 of SI) for subsequent 2D spectra. Among all local maxima, Δ values of 60 and 100 μs show the best cross peak intensity. Even though the optimal transfer conditions are narrow, optimization is relatively simple and straightforward.

Similar kinds of optimization were pursued using band-selective soft pulses in the aliphatic region instead of hard pulses. The variation of cross-peak intensity as a function of the delay Δ is shown in Figure S4. Whereas multiple-bond transfer efficiencies are relatively weak compared to hard-pulse MOCCA, use of soft pulses yields effective one-bond transfers. This provides evidence that MOCCA does not necessarily require hard pulses.

Not claiming to be complete, we compared the cross-peak buildup behavior of the MOCCA scheme with other exemplary recoupling sequences suitable for deuterated proteins at fast MAS. In particular, we characterized the relative performance of RFDR, TOBSY and MOCCA hard-pulse and soft-pulse mixing schemes. All the spectra were recorded using the pulse scheme depicted in Fig. 1 and under similar conditions, i.e., at 25 kHz spinning and in the absence of proton and deuterium decoupling. The offset was set to 56 ppm to quantify the magnetization transfer efficiency in the aliphatic region. To evaluate the transfer performance for different mixing sequences, we plotted the peak height of well-resolved peaks of the 2D

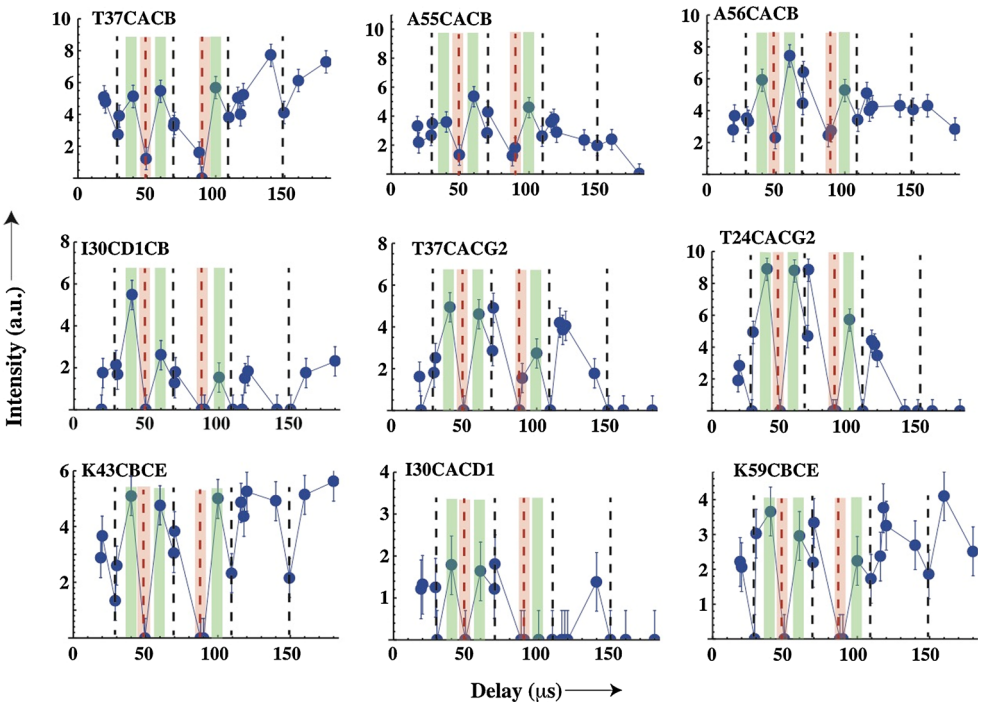

Fig. 2 Experimental optimization of MOCCA for multiple-bond transfer. Variation of cross-peak intensity of one- (*top row*), two- (*middle row*) and three-bond (*bottom row*) magnetization transfer as a function of the delay "Δ" between the 180° pulses during mixing. Total mixing time in all experiments was set to ~15 ms. Maximum and minimum of the magnetization efficiency transfer (for one-, two- and three-bond transfer simultaneously) are shown in *green* and *red* colors respectively. RFDR conditions, corresponding to $\Delta + \tau_{180°} = 1\tau_r$, $2\tau_r$, $3\tau_r$, and $4\tau_r$ are shown by the *black dashed lines*. Delays that accord to the 1.5 and 2.5 τ_r conditions are shown by *red dashed lines*

^{13}C–^{13}C spectra as a function of mixing time, see Fig. 3. The delay Δ and the duration of the 180-degree pulse in the MOCCA sequence were fixed to 60 and 10.5 µs, respectively, whereas for RFDR, these values were 29.5 and 10.5 µs to provide rotor-synchronized pulsing at 25 kHz spinning. For TOBSY, we used tangential shapes with an optimized duration of 28 µs without any spacing in between the pulses. In Fig. 3 and Figure S3 (SI), the corresponding intensities in the four different experiments are reported demonstrating examples of magnetization transfer efficiency for one-, two-, and three-bond transfer. We employed mixing up to maximum mixing times of 48, 19.2 and 11.4 ms for MOCCA hard pulse, RFDR, and TOBSY, respectively. These margins represent the maximum values up to which we felt comfortable in terms of sample and hardware integrity (with respect to the amount of total energy dissipated into the sample and the fraction of rf irradiation per time). While one-bond magnetization transfer is elicited with similar efficiency in all mixing sequences employed, significant differences are observed for longer-range mixing. The two- and three- bond transfers observed are most likely elicited by relayed transfer, even though transfer mediated by the smaller 2- and 3-bond *J* couplings is also theoretically possible. Relatively strong cross-peak signal intensity from hard-pulse MOCCA can be observed for two- and three-bond magnetization transfers. RFDR performs second best after hard pulse MOCCA under the chosen conditions. Both TOBSY and soft-pulse

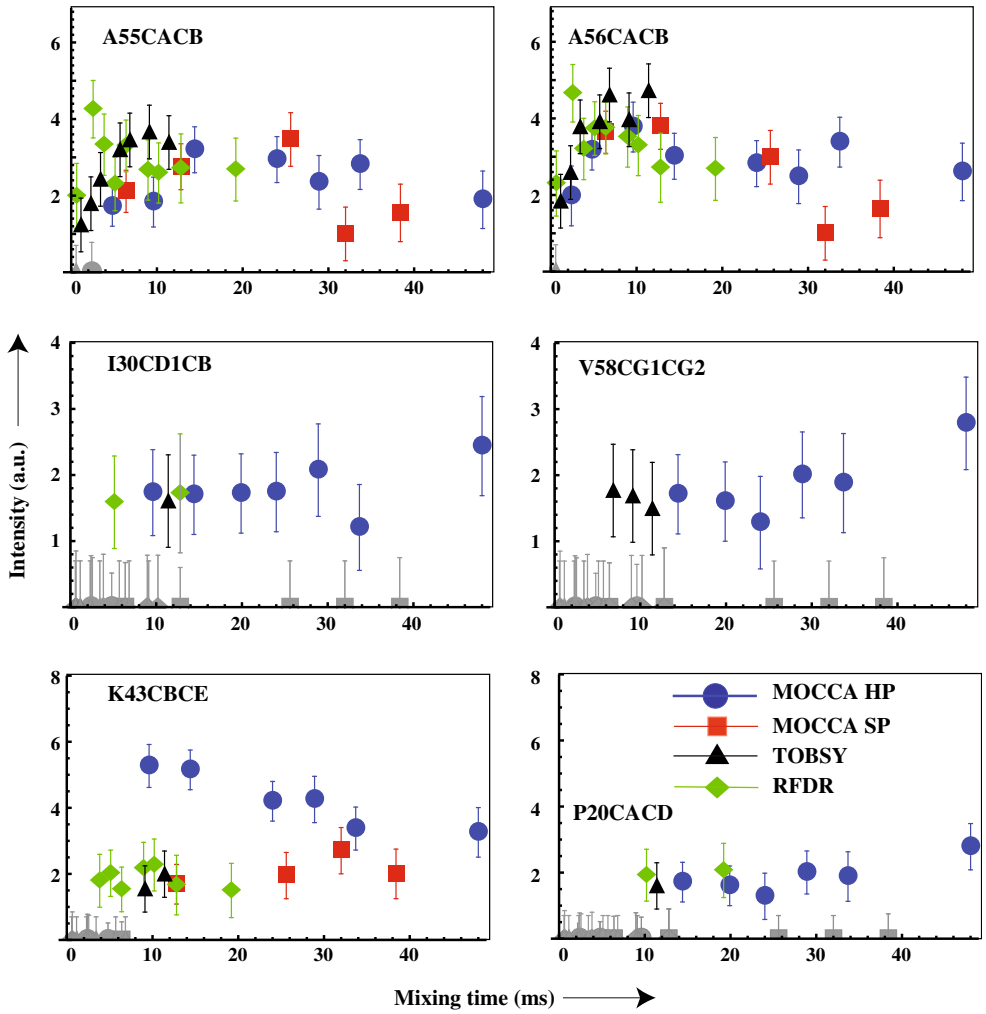

Fig. 3 Carbon-carbon transfer efficiency of MOCCA soft pulse (*red squares*), RFDR (*green diamonds*), MOCCA hard pulse (*blue spheres*), and TOBSY (*black triangles*) as a function of mixing time. A series of 2D ^{13}C–^{13}C spectra was recorded on the SH3 domain with different isotropic mixing periods. The signal intensity for one- (*top row*), two- (*middle row*), and three-bond magnetization transfer (*bottom row*) is plotted for representative examples as a function of the ^{13}C–^{13}C mixing time. The RF pulse amplitudes during carbon–carbon mixing using MOCCA soft pulse and TOBSY were 5 and 37 kHz, respectively. For MOCCA and RFDR, the RF pulse strength was 47.6 kHz. The delay in MOCCA hard pulse was set to 60 µs. For this comparison processing parameters were kept identical. Some data points, particularly those reflecting the short mixing times, have low intensities and are below the noise level. When they could not be reliably peak picked, they appear at zero values in the plot and are colored in *gray*

MOCCA show low transfer efficiency for 2- and 3-bond magnetization transfer. MOCCA hard pulse does not provide the magnetization transfer to carbonyl carbons under these conditions, which is in contrast to RFDR and TOBSY. For hard pulse MOCCA, a mixing time of 30–40 ms is optimal for full side-chain assignment.

Figure 4 shows the 2D carbon–carbon correlation experiments with parameters optimized to provide long-range mixing performance for all the above-mentioned mixing sequences. For visual clarity, some of the assigned peaks are shown. Cleary, hard pulse MOCCA shows excellent performance in terms of long-range transfers. To quantify the performance of these sequences, representative crosspeak-to-diagonal-ratio values for two residues are shown in Table 1.

Discussion

We find that MOCCA isotropic mixing performs well for deuterated proteins, where a dense proton network is absent and mixing sequences like PDSD and DARR would not work. In contrast to most rotor-synchronized mixing schemes, MOCCA introduces relatively low levels of energy into the sample even for fast MAS, since the number of pulses per time is independent of the rotor period. At 25 kHz,

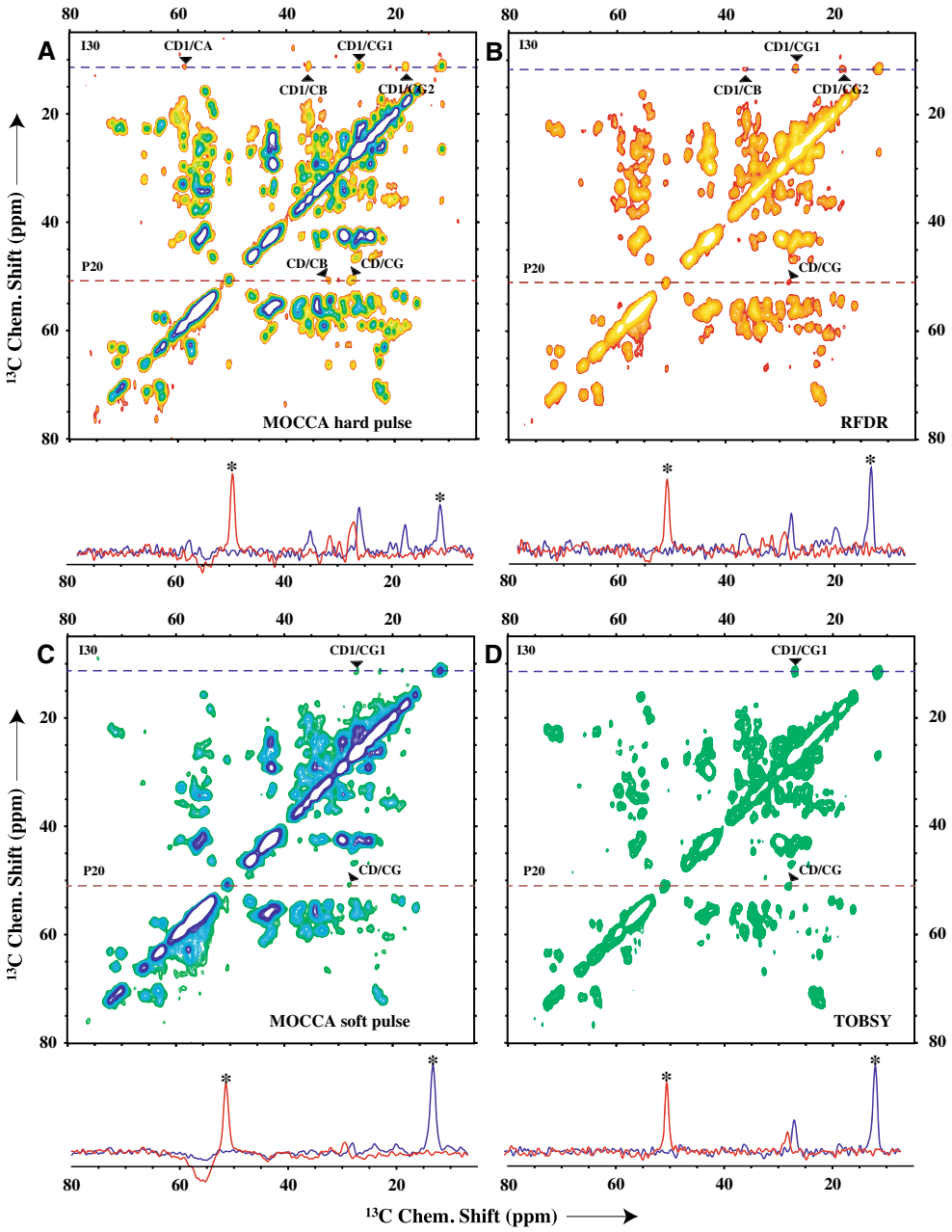

Fig. 4 Carbon-carbon correlation spectra with optimized experimental parameters for **a** hard-pulse MOCCA **b** RFDR **c** soft-pulse MOCCA, and **d** TOBSY mixing sequences. Their corresponding 1D (for P20, *red*, and I30, *blue*) slices are shown below each figure. Diagonal peaks are marked with an *asterisk*. All spectra were processed with identical processing parameters and plotted with similar contour levels. The phasing of the soft-pulse MOCCA is difficult to achieve. Mixing times of 30, 20, 25 and 10 ms were used for MOCCA hard pulse, RFDR, soft-pulse MOCCA and TOBSY, respectively. Each spectrum was recorded in 12 h

Table 1 Comparison of transfer efficiencies of various mixing sequences using two 1D cross sections corresponding to chemical shifts δ of 11.1 and 50.7 ppm (Fig. 4)

Pulse sequence	Amino acid	Cross peak/ diagonal peak (%)	One-bond transfer (%)	Two-bond transfer (%)	Three-bond transfer (%)	Diagonal peak, s/n (%)
RFDR	ILE 30	47 (± 6)	23 (± 6)	14 (± 8)	10 (± 4)	46 (± 5)
	PRO 20	21 (± 3)	21 (± 3)	–	–	64 (± 9)
MOCCA hard pulse	ILE 30	69 (± 4)	29 (± 4)	14.3 (± 4)	7.2 (± 4); 18 (± 4)	89 (± 12)
	PRO 20	37 (± 5)	24 (± 5)	13 (± 5)	–	95 (± 8)
MOCCA soft pulse	ILE 30	10 (± 5)	10 (± 5)	–	–	60 (± 4)
	PRO 20	12 (± 5)	12 (± 5)	–	–	86 (± 5)
TOBSY	ILE 30	30 (± 4)	30 (± 4)	–	–	100 (± 10)
	PRO 20	23 (± 6)	23 (± 6)	–	–	100 (± 10)

The total transfer efficiencies (The third column refers to the sum of cross peak intensities for a given residue) as well as transfer efficiencies for one, two and three bonds are given. All transfer efficiencies are calculated as % of the diagonal peaks at δ of 11.1 and 50.7 ppm, respectively, from a ^{13}C–^{13}C 2D spectrum. MOCCA hard pulse shows the highest overall transfer efficiency for aliphatic carbons. The RFDR performance is the second best after hard pulse MOCCA. TOBSY performs better than MOCCA soft pulse

the optimal spacing is on the order of 60 μs between two hard 180-degree pulses (10.5 μs), which represents a factor of almost two at 25 kHz MAS compared with RFDR. If we deliberately assume a limit of 7 ms continuous high-power ^{13}C irradiation (50 kHz), this enables mixing periods of up to 50 ms or longer for MOCCA versus roughly 25 ms for RFDR. For 65 kHz MAS, this calculation would result in roughly 10 ms RFDR. Then (with a rotor period of 15 μs) the pulses would usually be chosen significantly shorter than 10 μs. This would represent deposition of even more energy per time and the mixing times would usually be reduced even further for the sake of sample integrity. In addition, precise regulation of spinning speed and rotor synchronization at these spinning rates is more challenging mechanically, and the asynchronous MOCCA sequence may be beneficial.

A reason for the better performance of the isotropic mixing scheme MOCCA for long-range transfers relative to RFDR mixing might be due to dipolar truncation effects. These are expected to affect the dipolar-based mixing schemes in a more detrimental way than *J*-based sequences. The weaker performance of TOBSY, which we employed in its non-rotor-synchronized *J*-based version for long-range transfers, may be due to our conservative limitations in terms of energy deposition (12 ms mixing with 50 kHz adiabatic pulses). This limit is a consequence of the continuous, relatively strong rf irradiation for this TOBSY scheme as opposed to the interrupted rf pulses upon MOCCA.

Since MOCCA does not necessarily require hard pulses, it might further be tested with respect to reduced excitation profiles only, which would permit applications like three-bond sequential transfer as Cα–Cα or C′–C′. (Takeuchi et al. 2011) Also, shaped pulses with multiple excitation regions could be tried to recouple spins in very different spectral regions, like carbonyl and aliphatic nuclei at high magnetic field strengths. This might be of more interest if the available magnetic fields increase further.

In general, the low power requirements of the non-rotor-synchronized MOCCA scheme seem a highly valuable feature particularly in the light of increasing MAS speeds. Both the shorter pulse lengths required for pulses in most rotor-synchronized schemes and the increasing number of pulses per time, as well as the ν_r-dependent power requirements of many C-or R-sequences (Hohwy et al. 1998; Hou et al. 2011; Kristiansen et al. 2006; Levitt 2002) represent significant hurdles that we do not find using MOCCA.

In addition to the non-rotor-synchronized MOCCA, also low-power symmetry-based mixing sequences including low-power TOBSY, which may reduce the heat dissipation associated with the common TOBSY schemes, are being sought as alternatives to the traditional mixing sequences. (Herbst et al. 2011; Bellstedt et al. 2012; Nielsen et al. 2011; Teymoori et al. 2013) Given that each of the various mixing sequences has their advantages and limitations, simulation studies of the increasing number of existing schemes could help finding general guidelines for their use in upcoming biological and chemical projects.

Conclusion

To conclude, we demonstrated that liquid-state isotropic through-bond mixing sequences like MOCCA can be applied to perdeuterated proteins under magic-angle spinning conditions. We compared this mixing sequence with existing carbon–carbon mixing sequences. We optimized MOCCA for through-bond transfer with soft and hard 180-degree pulses. Soft-pulse MOCCA is efficient for

peaks in restricted regions of the spectrum. Hard-pulse MOCCA shows good magnetization transfer efficiency through many bonds and gives intense peaks in comparison to RFDR and TOBSY sequences, looking at the aliphatic region of the spectrum. The soft-pulse version might be useful for more specific applications like three-bond sequential transfer or overcoming difficulties associated with the large spectral widths at high fields. Due to a small ratio of the 180° pulse length to the delay between pulses, this type of mixing can be very useful for longer mixing times with reduced heating of the sample. This advantage will be exploited at ultra-fast MAS spinning speeds with shorter rotor periods. Given the simplicity of the sequence, the experimental setup is easy and straightforward, which provides a good alternative to the common homonuclear mixing schemes.

Acknowledgments We are thankful to Brigitta Angerstein for technical assistance. RL acknowledges support from the Max Plank Gesellschaft, from the Deutsche Forschungsgemeinschaft (Emmy Noether Program and SFB 803, project A04), and the Verband der Chemischen Industrie (VCI) in terms of a Liebig junior group fellowship.

References

Agarwal V, Reif B (2008) Residual methyl protonation in perdeuterated proteins for multi-dimensional correlation experiments in MAS solid-state NMR spectroscopy. J Magn Reson 194:16–24

Agarwal V, Diehl A, Skrynnikov N, Reif B (2006) High resolution ^{1}H detected ^{1}H,^{13}C correlation spectra in MAS solid-state NMR using deuterated proteins with selective ^{1}H,^{2}H isotopic labeling of methyl groups. J Am Chem Soc 128:12620–12621

Agarwal V et al (2014) De novo 3D structure determination from submilligram protein samples by solid-state 100 kHz MAS NMR spectroscopy. Angew Chem Int Ed 53:12253–12256

Akbey U, Oschkinat H, van Rossum BJ (2009) Double-nucleus enhanced recoupling for efficient ^{13}C MAS NMR correlation spectroscopy of perdeuterated proteins. J Am Chem Soc 131:17054

Asami S, Schmieder P, Reif B (2010) High resolution ^{1}H-detected solid-state NMR spectroscopy of protein aliphatic resonances: access to tertiary structure information. J Am Chem Soc 132:15133–15135

Asami S, Porter JR, Lange OF, Reif B (2015) Access to Cα backbone dynamics of biological solids by ^{13}C T_1 relaxation and molecular dynamics simulation. J Am Chem Soc 137:1094–1100

Baldus M, Meier BH (1996) Total correlation spectroscopy in the solid state. The use of scalar couplings to determine the through-bond connectivity. J Magn Reson Ser A 121:65–69

Barbet-Massin E et al (2014) Rapid proton-detected NMR assignment for proteins with fast magic angle spinning. J Am Chem Soc 136:12489–12497

Bellstedt P, Herbst C, Häfner S, Leppert J, Görlach M, Ramachandran R (2012) Solid state NMR of proteins at high MAS frequencies: symmetry-based mixing and simultaneous acquisition of chemical shift correlation spectra. J Biomol NMR 54:325–335

Bennett AE, Ok JH, Griffin RG, Vega S (1992) Chemical-shift correlation spectroscopy in rotating solids–radio frequency-driven dipolar recoupling and longitudinal exchange. J Chem Phys 96:8624–8627

Bennett AE, Rienstra CM, Griffiths JM, Zhen WG, Lansbury PT, Griffin RG (1998) Homonuclear radio frequency-driven recoupling in rotating solids. J Chem Phys 108:9463–9479

Bloembergen N (1949) On the interaction of nuclear spins in a crystalline lattice. Physica 15:386–426

Brinkmann A, Eden M, Levitt MH (2000) Synchronous helical pulse sequences in magic-angle spinning nuclear magnetic resonance: double quantum recoupling of multiple-spin systems. J Chem Phys 112:8539–8554

Carravetta M, Eden M, Zhao X, Brinkmann A, Levitt MH (2000) Symmetry principles for the design of radiofrequency pulse sequences in the nuclear magnetic resonance of rotating solids. Chem Phys Lett 321:205–215

Chevelkov V, Rehbein K, Diel A, Reif B (2006) Ultra-high resolution in proton solid-state NMR spectroscopy at high levels of deuteration. Angew Chem Int Ed 45:3878–3881

Chevelkov V, Faelber K, Schrey A, Rehbein K, Diehl A, Reif B (2007) Differential line broadening in MAS solid-state NMR due to dynamic interference. J Am Chem Soc 129: 10195–10200

Chevelkov V, Fink U, Reif B (2009) Accurate determination of order parameters from ^{1}H,^{15}N dipolar couplings in MAS solid-state NMR experiments. J Am Chem Soc 131:14018–14022

de Boer I et al (2004) MAS NMR structures of aggregated cadmium chlorins reveal molecular control of self-assembly of chlorosomal bacteriochlorophylls. J Phys Chem B 108:16556–16566

Felli IC, Pierattelli R, Glaser SJ, Luy B (2009) Relaxation-optimised Hartmann–Hahn transfer using a specifically Tailored MOCCA-XY16 mixing sequence for carbonyl-carbonyl correlation spectroscopy in ^{13}C direct detection NMR experiments. J Biomol NMR 43:187–196

Goddard TD, Kneller DG SPARKY 3, University of California, San Francisco

Grzesiek S, Bax A (1995) Spin-locked multiple quantum coherence for signal enhancement in heteronuclear multidimensional NMR experiments. J Biomol NMR 6:335–339

Hardy EH, Verel R, Meier BH (2001) Fast MAS total through-bond correlation spectroscopy. J Magn Reson 148:459–464

Herbst C, Herbst J, Leppert J, Ohlenschläger O, Görlach M, Ramachandran R (2011) Chemical shift correlation at high MAS frequencies employing low-power symmetry-based mixing sequences. J Biomol NMR 50:277–284

Hohwy M, Jacobsen HJ, Edén M, Levitt MH, Nielsen NC (1998) Broadband dipolar recoupling in the nuclear magnetic resonance of rotating solids: a compensated C_7 pulse sequence. J Chem Phys 108:2686–2694

Hou G, Byeon I-JL, Ahn J, Gronenborn AM, Polenova T (2011) ^{1}H–^{13}C/^{1}H–^{15}N heteronuclear dipolar recoupling by R-symmetry sequences under fast magic angle spinning for dynamics analysis of biological and organic solids. J Am Chem Soc 133:18646–18655

Hou G, Byeon IJ, Ahn J, Gronenborn AM, Polenova T (2012) Recoupling of chemical shift anisotropy by R-symmetry sequences in magic angle spinning NMR spectroscopy. J Chem Phys 137:134201

Huber M, Hiller S, Schanda P, Ernst M, Böckmann A, Verel R, Meier BH (2011) A proton-detected 4D solid-state NMR experiment for protein structure determination. J Chem Phys 12:915–918

Huber M, Böckmann A, Hiller S, Meier BH (2012) 4D solid-state NMR for protein structure determination. Phys Chem Chem Phys 14:5239–5246

Kadkhodaie M, Rivas O, Tan M, Mohebbi A, Shaka AJ (1991) Broadband homonuclear cross polarization using flip-flop spectroscopy. J Magn Reson 91:437–443

Knight MJ et al (2011) Fast resonance assignment and fold determination of human superoxide dismutase by high-resolution

proton-detected solid-state MAS NMR spectroscopy. Angew Chem Int Ed 50:11697–11701

Knight MJ et al (2012) Structure and backbone dynamics of a microcrystalline metalloprotein by solid-state NMR. Proc Natl Acad Sci USA 109:11095–11100

Kramer F, Peti W, Griesinger C, Glaser SJ (2001) Optimized homonuclear Carr-Purcell-type dipolar mixing sequences. J Magn Reson 149:58–66

Kristiansen PE, Carravetta M, Beek JDv, Lai WC, Levitt MH (2006) Theory and applications of supercycled symmetry-based recoupling sequences in solid-state NMR. J Chem Phys 124: 234510–234519

Lamley JM et al (2014) Solid-state NMR of a protein in a precipitated complex with a full-length antibody. J Am Chem Soc 136: 16800–16806

Leppert J, Ohlenschlager O, Gorlach M, Ramachandran R (2004) Adiabatic TOBSY in rotating solids. J Biomol NMR 29:167–173

Levitt MH (2002) Symmetry-based pulse sequences in magic-angle spinning solid-state NMR. In: Grant DM, Harris RK (eds) Encyclopedia of Nuclear Magnetic Resonance, Advances in NMR, vol 9. Wiley, Chichester, pp 165–196

Lewandowski JR, Dumez J-N, Akbey U, Lange S, Emsley L, Oschkinat H (2011) Enhanced resolution and coherence lifetimes in the solid-state NMR spectroscopy of perdeuterated proteins under ultrafast magic-angle spinning. J Phys Chem Lett 2:2205–2211

Linser R (2011) Side-chain to backbone correlations from solid-state NMR of perdeuterated proteins through combined excitation and long-range magnetization transfers. J Biomol NMR 51:221–226

Linser R, Chevelkov V, Diehl A, Reif B (2007) Sensitivity enhancement using paramagnetic relaxation in MAS solid-state NMR of perdeuterated proteins. J Magn Reson 189:209–216

Linser R, Fink U, Reif B (2008) Proton-detected scalar coupling based assignment strategies in MAS solid-state NMR spectroscopy applied to perdeuterated proteins. J Magn Reson 193:89–93

Linser R, Fink U, Reif B (2009) Probing surface accessibility of proteins using paramagnetic relaxation in solid-state NMR spectroscopy. J Am Chem Soc 131:13703–13708

Linser R, Fink U, Reif B (2010) Assignment of dynamic regions in biological solids enabled by spin-state selective NMR experiments. J Am Chem Soc 132:8891–8893

Linser R, Bardiaux B, Higman V, Fink U, Reif B (2011a) Structure calculation from unambiguous long-range amide and methyl ^{1}H-^{1}H distance restraints for a micro-crystalline protein with MAS solid state NMR. J Am Chem Soc 133:5905–5912

Linser R et al (2011b) Proton detected solid-state NMR of fibrillar and membrane proteins. Angew Chem Int Ed 50:4508–4512

Linser R, Bardiaux B, Hyberts SG, Kwan AH, Morris VK, Sunde M, Wagner G (2014) Solid-state NMR structure determination from diagonal-compensated, sparsely nonuniform-sampled 4D proton–proton restraints. J Am Chem Soc 136:11002–11010

McDermott AE, Creuzet FJ, Kolbert AC, Griffin RG (1992) High-resolution magic-angle-spinning NMR spectra of protons in deuterated solids. J Magn Reson 98:408–413

Morcombe CR, Paulson EK, Gaponenko V, Byrd RA, Zilm KW (2005) ^{1}H-^{15}N correlation spectroscopy of nanocrystalline proteins. J Biomol NMR 31:217–230

Nielsen NC, Creuzet F, Griffin RG, Levitt MH (1992) Enhanced double-quantum nuclear-magnetic-resonance in spinning solids at rotational resonance. J Chem Phys 96:5668–5677

Nielsen AB, Jain SK, Nielsen NC (2011) Low-power homonuclear dipolar recoupling using supercycled symmetry-based and exponentially-modulated pulse sequences. Chem Phys Lett 503:310–315

Schanda P, Meier BH, Ernst M (2010) Quantitative analysis of protein backbone dynamics in microcrystalline ubiquitin by solid-state NMR spectroscopy. J Am Chem Soc 132:15957–15967

Takegoshi K, Nakamura S, Terao T (2001) ^{13}C-^{1}H dipolar-assisted rotational resonance in magic-angle spinning NMR. Chem Phys Lett 344:631–637

Takeuchi K, Gal M, Takahshi H, Shimada I, Wagner G (2011) HNCA-TOCSY-CANH experiments with alternate (13)C-(12)C labeling: a set of 3D experiment with unique supra-sequential information for mainchain resonance assignment. J Biomol NMR 49:17–26

Teymoori G, Pahari B, Viswanathan E, Eden M (2013) Multiple-quantum spin counting in magic-angle-spinning NMR via low-power symmetry-based dipolar recoupling. J Magn Res 236:31–40

Verel R, Baldus M, Ernst M, Meier BH (1998) A homonuclear spin-pair filter for solid-state NMR based on adiabatic-passage techniques. Chem Phys Lett 287:421–428

Verel R, Ernst M, Meier BH (2001) Adiabatic dipolar recoupling in solid-state NMR: the dream scheme. J Magn Reson 150:81–99

Yoshimura Y, Kulminskaya NV, Mulder FA (2015) Easy and unambiguous sequential assignments of intrinsically disordered proteins by correlating the backbone ^{15}N or ^{13}C' chemical shifts of multiple contiguous residues in highly resolved 3D spectra. J Biomol NMR 61:109–121